Random walks and magnetic oscillations in compensated metals

Jean-Yves Fortin[1,*] and Alain Audouard[2,†]

[1]*Institut Jean Lamour, Département de Physique de la Matière et des Matériaux, Groupe de Physique Statistique, CNRS–Nancy-Université, BP 70239, F-54506 Vandoeuvre les Nancy Cedex, France*

[2]*Laboratoire National des Champs Magnétiques Intenses (UPR 3228 CNRS, INSA, UJF, UPS), 143 Avenue de Rangueil, F-31400 Toulouse, France*

(Received 6 May 2009; revised manuscript received 5 November 2009; published 8 December 2009)

The field- and temperature-dependent de Haas-van Alphen oscillations spectrum is studied for an ideal two-dimensional compensated metal whose Fermi surface is made of a linear chain of successive orbits with electron and hole character, coupled by magnetic breakdown. We show that the first harmonic amplitude can be accurately evaluated on the basis of the Lifshits-Kosevich semiclassical formula by considering a set of random walks on the orbit network, in agreement with the numerical resolution of Pippard equations associated with the surface. Oppositely, the second-harmonic amplitude does not follow the Lifshits-Kosevich behavior and vanishes at a critical value of the field-to-temperature ratio which depends explicitly on the relative value between the hole and electron effective masses.

DOI: 10.1103/PhysRevB.80.214407 PACS number(s): 71.18.+y, 71.20.Rv, 74.70.Kn

I. INTRODUCTION

Due to their rather simple Fermi surface, organic metals provide a powerful playground for the investigation of quantum-oscillation physics. In that respect, the most well known example is provided by κ-(BEDT-TTF)$_2$Cu(NCS)$_2$ which can be regarded as the experimental realization of the Fermi surface considered by Pippard in the early 1960s for his model.[1] In the extended zone scheme, such a Fermi surface is composed of closed hole orbits and quasi-one-dimensional (1D) sheets, with gaps separating the holes bands from these sheets. Since these gaps are small compared with the Fermi energy, magnetic breakdown can develop as magnetic field increases. The tunneling probability amplitude p is function of the internal field B via the relation $p^2=e^{-B_0/B}$, where B_0 is the breakdown field which depends on the Fermi-surface geometry (see, for example, Chambers formula[2] or more generally Refs. 3 and 4 for a topological point of view). By including this effect in the semiclassical oscillations spectrum of Lifshits-Kosevich (LK), Falicov and Stachowiak[5] developed a theory based on the Green's-function formalism in order to evaluate exactly the Fourier amplitudes of the oscillating part of the magnetization. Indeed, the knowledge of the Green's function for wave packets traveling along closed and classical orbits on the Fermi surface leads directly to the quasiparticle density of states. In particular, the amplitudes are expressed as a sum over all classical orbits allowed on the network by using only tunneling rules. However, the above-mentioned type of Fermi surface yields quantum-oscillations spectra with numerous frequency combinations that cannot be accounted for by this semiclassical model. This phenomenon which has raised a great interest[6–12] is generally attributed to either the formation of Landau bands or (and) oscillations of the chemical potential in magnetic field.

Beside the observation of frequency combinations, strong deviations of the field and temperature dependence of both the first- and second-harmonics amplitude are observed in few α-phase BEDT-TTF salts.[13,14] Even though the Fermi-surface topology of α- and κ-phases salts is similar, the salient feature of the former is their very large magnetic breakdown gap. As a result, the quasi-1D sheets can be regarded as electron reservoirs and the resulting magnetization data were interpreted on the basis of a quasi-1D density of states-dependent oscillation of the chemical potential.[15,16]

Contrary to the above-mentioned examples, the Fermi surface of numerous organic metals is composed of compensated electron- and hole-type closed orbits,[17] yielding many frequency combinations as well, as far as Shubnikov-de Haas oscillations are concerned.[18–20] In the case of a Fermi surface composed of two compensated orbits coupled to each other through magnetic breakdown but isolated from the other orbits outside the first Brillouin zone, it has been shown that the oscillations of the chemical potential can be strongly damped[21] which could account for the absence of frequency combinations reported in the de Haas-van Alphen (dHvA) spectra of two-dimensional (2D) networks of compensated orbits in fields up to 28 T.[20] However, the Fermi surface considered in Ref. 21 which, to our knowledge, has no counterpart among the compounds synthesized up to now, does not provide a network of orbits and, therefore, do not yield Landau bands in magnetic field.

The aim of this paper is to explore the field and temperature dependence of the dHvA oscillations spectra of an ideal 2D metal whose Fermi surface achieves a linear chain of successive electron- and hole-type compensated orbits with no reservoir of electron. Such a topology can be relevant in compounds for which the Fermi surface originates from an orbit with an area equal to that of the first Brillouin zone and coming close to the boundary along one direction, as it has been predicted for (BEDT-TTF)$_4$NH$_4$[Fe(C$_2$O$_4$)$_3$].C$_3$H$_7$NO.[22] In this case, a large magnetic breakdown gap is observed at this point and a linear chain of successive electron-hole tubes separated with a smaller magnetic breakdown gap can be observed. Analogous topology is also realized in the Bechgaard salt (TMTSF)$_2$NO$_3$ in the temperature range in between the anion ordering temperature and the spin-density wave condensation[23] (see Fig. 1). We will focus on the field- and

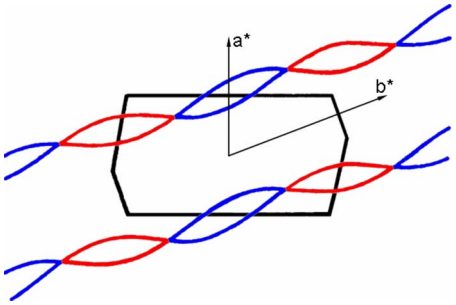

FIG. 1. (Color online) Calculated Fermi surface of the Bechgaard salt $(TMTSF)_2NO_3$ in the temperature range below the anion ordering and above the spin-density wave condensation, according to Ref. 23. Solid blue, centered at $(a^*,0)$ and red centered at (a^*,b^*), lines are compensated hole and electron orbits, respectively.

temperature-dependent amplitude of the first and second harmonics A_1 and A_2 of the oscillatory part of the magnetization M_{osc}, derived for such Fermi-surface topology, which can be expanded as $M_{osc}=\Sigma_n(-1)^n A_n \sin(2\pi n F_0/b)$, where the fundamental frequency of the problem F_0 and the dimensionless magnetic field b are specified in the next section. It is shown that A_1 is nicely accounted for by the Lifshits-Kosevich formula, provided the summation over all possible paths contributing to the main frequency is considered. Oppositely, in the case where the effective masses linked to the electron and hole orbits are different, strong deviations from the Lifshits-Kosevich formula can be observed for A_2 which vanishes at a field value depending on the ratio of the two effective masses, only, irrelevant to the magnetic breakdown field value.

II. MODEL

We consider a 2D metal whose electronic structure consists of two parabolic bands with hole and electron character yielding a periodic array of compensated orbits (see Fig. 2). The bottom of the electron band is set at zero energy while the top of the hole band is at $\Delta>0$ with the possibility for the quasiparticle to tunnel through a gap between two successive orbits by magnetic breakdown. The total number of quasiparticles in the system is constant and, to lower the total energy at zero field and zero temperature, the area of the hole band at the Fermi surface should be equal to the area of the electron band which accounts for compensation. Indeed, if the hole band were completely filled, the zero-field energy would be higher than if part of the quasiparticles were transferred from the hole band to the electron band. In the following, the effective masses linked to the two bands, m_e^* and m_h^*, can be different. As in Refs. 12 and 21, the dimensionless field b and temperature t are given by $b=B/\tilde{B}$ and $t=T/\tilde{T}$, respectively, where $\tilde{B}=h/eA_0$, $\tilde{T}=\tilde{E}/k_B$, and A_0 is the unit cell area. The effective masses and energies are expressed in free-electron mass m_0 units and in units of $\tilde{E}=2\pi\hbar^2 m_0 A_0$, respectively. Unit-cell area of most organic metals is in the range 100–200 $Å^2$ yielding $\tilde{B}$ and $\tilde{T}$ values of few thousands of teslas and kelvins, respectively. Therefore, realistic experimental conditions yield small values of b and t compared to $\tilde{B}$ and $\tilde{T}$, respectively. On the contrary, the ratio b/t, which is the relevant external parameter for perfect crystals, is given by $b/t=(e\hbar/m_0k_B)\,B/T$. Its value is close to the B/T ratio achieved in experiments since $e\hbar/m_0k_B\simeq 1.34$ K T^{-1}. Given an energy E, the areas of the electron- and hole-type surfaces are, respectively, $S_e=2\pi m_e^* E$ and $S_h=2\pi m_h^*(\Delta-E)$, which are both quantized for closed orbits in the Brillouin zone. The zero-field Fermi energy μ_0 is given by the condition of compensation $S_e(\mu_0)=S_h(\mu_0)$ hence $\mu_0=m_h^*\Delta/(m_e^*+m_h^*)$. The fundamental frequency of this system is therefore equal to $F_0=S_e(\mu_0)/2\pi=S_h(\mu_0)/2\pi=m_e^*m_h^*\Delta/(m_e^*+m_h^*)$. Each Landau level has a degeneracy b per sample area. The spectrum of such chain of coupled electron-hole orbits and the quantization of the energy are determined by semiclassical and conservation rules of the wave-function amplitudes at the junctions where the quasiparticles tunnel and across the boundaries of the Brillouin zone. In particular, the amplitude of the wave function at different points of the Fermi surface (see Fig. 2 for notations) satisfies the following rules: its phase is proportional to the area swept by the quasiparticle around the trajectory divided by b. We will note $\sigma_e=S_e/2b$ and $\sigma_h=S_h/2b$ the phases around half the electron and hole orbits, respectively. Also, at every junction there is a probability ip for the quasiparticle to tunnel and a probability q to be reflected. Finally we add a Maslov index $i=\sqrt{-1}$ at the vertical extrema of the orbits (cross symbols on Fig. 2). With these rules, we can write the relations between the wave-function amplitudes α's and β's,

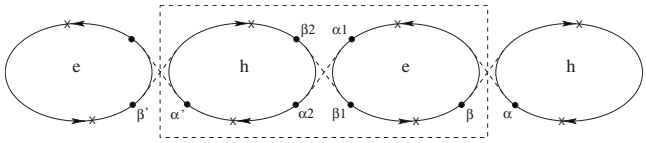

FIG. 2. One-dimensional chain of coupled electron and hole orbits. The first Brillouin zone is delimited by the dotted lines. Amplitudes are chosen at specific points on the trajectory (see text).

$$\alpha_1 = i\exp(i\sigma_e)(ip\alpha + q\beta),$$

$$\alpha_2 = ip\alpha_1 + q\beta_2, \quad \alpha' = i\exp(-i\sigma_h)\alpha_2$$

$$\beta_1 = q\alpha_1 + ip\beta_2, \quad \beta = i\exp(i\sigma_e)\beta_1$$

$$\beta_2 = i\exp(-i\sigma_h)(q\alpha' + ip\beta'). \tag{1}$$

As boundary conditions, we impose that the amplitudes across the first Brillouin zone are identical up to an arbitrary phase θ: $\alpha'=\alpha\exp(i\theta)$ and $\beta'=\beta\exp(i\theta)$. Solving this system of closed equations, we obtain the quantization of the energy which satisfies the spectrum equation

$$\begin{aligned}&[1+q^2\exp(2i\sigma_e)-p^2\exp i(\sigma_e-\sigma_h+\theta)]\\&\times[1+q^2\exp(-2i\sigma_h)-p^2\exp i(\sigma_e-\sigma_h-\theta)]\\&=-p^2q^2[\exp i(\sigma_e-\sigma_h)+\exp(-2i\sigma_h+i\theta)]\\&\times[\exp i(\sigma_e-\sigma_h)+\exp(2i\sigma_e-i\theta)].\end{aligned} \tag{2}$$

We can distinguish two limiting behaviors. For $q=1$ (or, equivalently, $p=0$), the spectrum reduces to $[1+\exp(2i\sigma_e)]\times[1+\exp(-2i\sigma_h)]=0$ which corresponds to the discrete Landau levels of two independent electron and hole orbits: $S_e(E_n)=2\pi b(n+1/2)$ and $S_h(E_n)=2\pi b(n+1/2)$, with n positive integer. In the opposite case where $q=0$, the spectrum corresponds to nonquantized phases $\sigma_e(E)-\sigma_h(E)=\pm\theta$ since no closed orbit exists in such case (open chain) and therefore magnetic oscillations vanish, leaving the place to a continuum of states. To study numerically the spectrum given by Eq. (2), we first determine the periodicity in energy of the discrete Landau levels. For that purpose, we assume that $m_h^*/m_e^*=q_0/p_0$, where q_0 and p_0 are coprime integers that can be as large as needed to approximate the ratio of the two masses. It is indeed useful to express this quantity with a rational number since it allows to consider as necessary only a finite set of solutions of Eq. (2). The minimal periodicity T_E of the spectrum is, in this case and for a given phase θ, equal to $T_E=2bp_0/m_e^*$, which is twice the periodicity calculated for an isolated system made of one hole and one electron band.[21] The number of solutions inside each interval of width T_E is found to be equal to $2(p_0+q_0)$ (this number is conserved when p varies and can be counted exactly for $p=0$). Given a set of solutions $E_{eh}(q,n,\theta)$, $n=0,\cdots,2(p_0+q_0)-1$, we introduce a cutoff function $\varphi_c(E)$ such as $\varphi_c(E)=1$ for E larger than a characteristic energy E_c and equal to $\exp[-c(E-E_c)^{2\delta}]$ for $E\leq E_c$, where δ is any positive integer greater than 1 (we take $\delta=4$ in the simulations which gives a very smooth cutoff function), and c a positive parameter determined self-consistently. This function has the property of preserving the physical features near the Fermi surface and the ground-state energy is, in particular, finite since now the corresponding hole spectrum is bounded for large and negative energies. The Landau-level density of states $\rho_c(E)$ takes the following form

$$\rho_c(E)=\frac{b}{2\pi}\int_0^{2\pi}d\theta\sum_{n=0}^{2(p_0+q_0)-1}\sum_{k=-\infty}^{\infty}\varphi_c(E)\delta\times[E-E_{eh}(q,n,\theta)-kT_E]. \tag{3}$$

Given E_c, the positive parameter c is found to be solution of the equation of conservation at zero temperature

$$N_{eh}=\int_{-\infty}^{\mu_0(b)}dE\rho_c(E)=\frac{b}{2\pi}\int_{-\infty}^{\mu_0(b)}dE\int_0^{2\pi}d\theta\sum_{n=0}^{p_0+q_0-1}\sum_{k=-\infty}^{\infty}\varphi_c(E)\delta\times[E-E_{eh}(q,n,\theta)-kT_E], \tag{4}$$

where N_{eh} is, as mentioned before, the total number of quasiparticles in the canonical ensemble. In the numerical simulations, $\mu_0(b)$ is taken as the first Landau level located below μ_0. We choose N_{eh}, which is arbitrary, as a multiple of the characteristic zero-field energy density $(m_e^*+m_h^*)\mu_0$ (which is proportional to the areas of the Fermi surface). We will also choose in the following $E_c=-2$ and $N_{eh}=8(m_e^*+m_h^*)\mu_0$, and 10 values of θ for the integral evaluations. For each value of the field b, the parameter c defined from Eq. (4) is unique and determined self-consistently. Then we can compute, for example, the ground-state energy ΔE_0

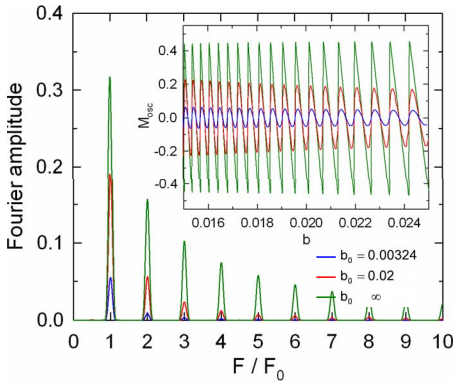

FIG. 3. (Color online) Fourier spectra of the oscillatory magnetization (displayed in the inset) for various values of the magnetic breakdown field b_0. The effective masses are $m_e=1$ and $m_h=2.5$. F_0 is the fundamental frequency (see text).

$$\Delta E_0=\frac{b}{2\pi}\int_{-\infty}^{\mu_0(b)}dE\int_0^{2\pi}d\theta\sum_{n=0}^{p_0+q_0-1}\sum_{k=-\infty}^{\infty}E\varphi_c(E)\delta\times[E-E_{eh}(q,n,\theta)-kT_E] \tag{5}$$

and the free-energy ΔF

$$\Delta F=-\frac{tb}{2\pi}\int_{-\infty}^{\infty}dE\int_0^{2\pi}d\theta\sum_{n=0}^{p_0+q_0-1}\sum_{k=-\infty}^{\infty}\varphi_c(E)\log\times[1+\exp\beta(\mu-E)]\delta[E-E_{eh}(q,n,\theta)-kT_E]+N_{eh}\mu. \tag{6}$$

The chemical potential $\mu=\mu(t,b)$ is calculated from Eq. (6) by extremizing the free energy $\partial\Delta F/\partial\mu=0$. The magnetization $M_{osc}=-\partial\Delta F/\partial b=x^2\partial\Delta F/\partial x$, where $x=1/b$, has to be independent of the parameter E_c for E_c far away from the chemical potential or at energies large compared to the Landau gap for a given magnetic field. We have checked, for different values of E_c with $\Delta=1$, for example, $E_c=-1,-2,-4$, and for a large range of fields, that the resulting magnetization is stable in this procedure.

Examples of field-dependent dHvA and chemical-potential oscillations deduced from the numerical resolution of Eq. (6) are given in Figs. 3 and 4, respectively. As evidenced in the inset of Fig. 4, the oscillations of the chemical potential are weaker than in the case of two electron bands (assuming same effective masses and same unique frequency). They even vanish in the case where $m_e^*=m_h^*$. As it will be discussed in Sec. IV and contrary to the case of two electron orbits, the chemical-potential oscillations for compensated orbits are linked to the difference between two temperature-dependent amplitudes. In the case where the effective masses (and the relaxation times for real crystals) of electron and hole orbits are the same, these amplitudes cancel each other and the chemical potential does not oscillate. It is due to the fact that the Landau levels of the quasielectrons and quasiholes are perfectly symmetric around the

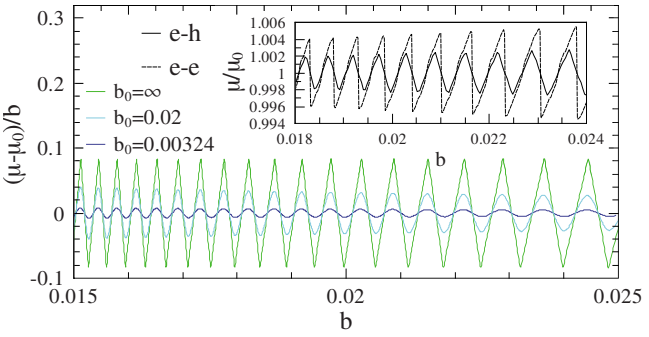

FIG. 4. (Color online) Field dependence of the chemical potential (μ) relatively to its value in zero field (μ_0) for various values of the magnetic breakdown field b_0 at $t=10^{-4}$. The effective masses are $m_e^*=1$ and $m_h^*=2.5$. The inset compares the ratio μ/μ_0 behavior for two compensated orbits (solid line) and two electron-type orbits (dashed line) of same area (or frequency) $F_0=5/7$ with effective masses $m_0^*=1$ and $m_1^*=2.5$, in the absence of magnetic breakdown ($b_0\to\infty$). The chemical potential for two electron orbits is computed from Ref. 12, Eq. (3) [see also Eq. (19) for the compensated orbit case], with the values (from this reference) $m_0^*=m_e^*=1$, $m_1^*=m_h^*=5/2$, and $\Delta_0=0$, $\Delta_1=\Delta(m_h^*-1)/(m_h^*+1)=3/7$.

zero-field Fermi energy since the masses are identical. Finally, Fig. 4 also shows that the oscillations decrease as magnetic breakdown develops. These features, which are in agreement with the conclusion derived for isolated orbits,[21] confirm that the field-dependent chemical-potential oscillations are damped in 2D compensated metals when compared to the uncompensated case. Nevertheless, as observed in Fig. 4, chemical-potential oscillations remain detectable if we consider the quantity $(\mu-\mu_0)/b$, which is the principal argument of the oscillating sine functions of the chemical potential [see below Eq. (19)], in particular, in the case where the magnetic breakdown field is large and the two effective masses strongly differ. Hence, the field and temperature dependence of the first- and second-harmonics amplitude are explored accordingly in the following. We will show that even though the first harmonics is almost not influenced by the chemical oscillations, these ones noticeably modify the features of the second harmonics.

III. AMPLITUDE OF THE FIRST HARMONIC WITHIN THE LIFSHITS-KOSEVICH THEORY USING RANDOM WALK ANALOGY

In this section, we compute the expression for the first-harmonic amplitude A_1^{LK}, corresponding to the frequency F_0, using the Lifshits-Kosevich and Falicov-Stachowiak theories based on the semiclassical calculation of all possible orbits in the network of closed orbits and contributing to this amplitude. We will check numerically that these two theories nicely account for the amplitude A_1 extracted from the spectrum computed numerically in the previous section. This has for important consequence that the Lifshits-Kosevich theory is accurately valid in most of field and temperature ranges for determining the first amplitude in the case of small oscillations of the chemical potential in this kind of Fermi surfaces. We first notice that there are an infinite number of orbits

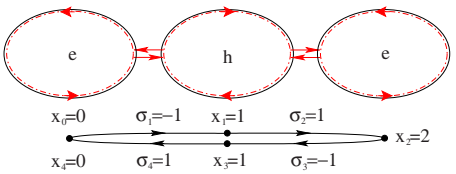

FIG. 5. (Color online) Example of a trajectory contributing to the first amplitude with fundamental frequency F_0 and mass $m_e(1)=2m_e^*+m_h^*$. The successive coordinates $\{x_i\}_{i=0,\ldots,4}$ of the quasiparticle are given below the figure. Here $n_i=0$ (see text). $\sigma_{-1}=-1$ since the particle is going backward when it is reaching the location $x_0=x_4$ from $x_{-1}=x_3$ on a periodic orbit.

along the chain contributing to this amplitude (see Ref. 21) since all the trajectories involving an odd number of orbits contribute to the frequency F_0. In contrast, an orbit involving an equal number of individual electron and hole orbits yields a zero frequency. Therefore, any orbit contributing to A_1 can be regarded as the sum of such a zero-frequency orbits combined with one electron or hole orbit. These orbits yielding the frequency F_0 can be classified by their successive masses $m_e(l)=lm_e^*+(l-1)m_h^*$ or $m_h(l)=(l-1)m_e^*+lm_h^*$, where l is a positive integer. The contribution of orbits with large effective mass is negligible at low field or high temperature (b/t small) but have a significant value in the large b/t limit where all the orbits have to be taken into account. Indeed the field- and temperature-dependent damping factors which are defined for a given set of effective masses $m_{e(h)}^*$ by the formula

$$R_T(m_{e(h)}^*)=\frac{2\pi^2 m_{e(h)}^* t/b}{\sinh(2\pi^2 m_{e(h)}^* t/b)} \tag{7}$$

are close to unity in this limit. Dingle factors

$$R_D(m_{e(h)}^*,t_{e(h)}^*)=\exp(-2\pi^2 m_{e(h)}^* t_{e(h)}^*/b), \tag{8}$$

where $t_{e(h)}^*=m_0A_0/4\pi^2\hbar\tau_{e(h)}$ are the reduced Dingle temperatures, can also be simply added as factor of the damping amplitudes R_T to account for real crystals in which the relaxation times $\tau_{e(h)}$ have finite values, so that the overall damping factor R can be written as

$$R(m_{e(h)}^*)=R_T(m_{e(h)}^*)R_D(m_{e(h)}^*,t_{e(h)}^*). \tag{9}$$

In the following we will assume first that these two relaxation times are negligibly small to simplify the calculations so that $R=R_T$. The existence of an infinite set of orbits contributing to the first harmonic leads us to define a closed random walk on the chain in the Brillouin zone $\{x_i\}_{i=0,2n}$, with origin and end at x_0 and x_{2n}, respectively, with the condition $x_0=x_{2n}=0$. These coordinates take integer values (either negative or positive) and define precisely the pocket inside which the quasiparticle is located. We chose x_i with i even to be the positions of the electron bands and i odd for the hole bands. A closed path has an even number of steps $2n$. For a given x_i, the particle can also orbit a number $n_i\geq 0$ of times around the surface before going to the next band. An example of a typical closed trajectory is given in Fig. 5.

We can rewrite coordinates x_i by the mean of forward/backward variables $\sigma_i = \pm 1$ such as $x_i = x_{i-1} + \sigma_i(x_{i-1} - x_{i-2})$. Here $\sigma_i = 1$ when the particle is going forward on its path (in the same direction) and $\sigma_i = -1$ when it is going backward in the reverse direction (see Fig. 5 for an explicit set of σ_i's). The path is moreover made periodic by imposing $x_i = x_{i\pm 2n}$ (just as for variables σ_i). On Fig. 5, $x_3 = x_{-1}$ and the particle is moving on the reverse direction when it is reaching the point $x_0 = x_4$ along the portion of path (x_{-1}, x_0, x_1), which implies that $\sigma_1 = -1$.

It will be also useful in the following to introduce new periodic variables $y_i = x_i - x_{i-1} = \pm 1$ which satisfy the simple relations $y_i = \sigma_i y_{i-1}$ and $\sigma_i = y_i y_{i-1}$. Let us now calculate the total number of possible orbits with a given effective mass $m_e(l)$ [or equivalently $m_h(l)$ for a hole orbit since the problem is symmetric by exchange of electron and hole masses] and their contribution to the amplitude of the first harmonic A_1^{LK} with the fundamental frequency F_0. If the particle is going forward, there is an amplitude equal to ip to be transmitted from one band to the next one or ipq if the particle is going backward (it has first to perform exactly one reflection with amplitude q on the band edge before being transmitted back through the previous junction). In term of variables σ_i, this is equivalent to write this partial amplitude as $ip[(1+\sigma_i)+(1-\sigma_i)q]/2 = ip\sqrt{q}e^{K\sigma_i}$, with $e^K = 1/\sqrt{q}$. Then the Lifshits-Kosevich amplitude corresponding to all electronlike contributions can be written as

$$A_1^{\mathrm{LK}}(e) = \frac{q^2 R(m_e^*)}{m_e^*} + \sum_{l\geq 2} \frac{R[m_e(l)]}{m_e(l)} \times \sum_{n=1}^{2(l-1)} \frac{1}{n} \sum_{\{n_i,\sigma_i\}} (-p^2)^n q^{n+2\Sigma_{j=0}^{2n-1} n_j} e^{K\Sigma_{i=1}^{2n}\sigma_i}. \quad (10)$$

The sum over l and $n \geq 1$ corresponds to all possible effective masses and number $(2n)$ of tunnelings, respectively. The first term $l=1$ in Eq. (10) is the simplest orbit of the expansion: a closed trajectory around one electron pocket with damping factor q^2 and effective mass m_e^*. The sum over n is limited to $2(l-1)$ which corresponds to the extremal trajectory. Indeed, for an orbit with effective mass $m_e(l)$, the quasiparticle visits a maximum of $(l-1)$ successive electron and hole pockets outside the first initial electron pocket before going back, $l-1$ being also the maximal linear extension of the path. This implies that all the n_i are zero for this case (see Fig. 5). The factor $1/n$ takes into account of the orbit symmetry by circular permutation of the coordinates $\{x_i\}$. Finally, the sum over the set $\{n_i, \sigma_i\}$ is constrained by the boundary conditions $x_0 = x_{2n}$ and by the facts that the frequency is set to F_0 and the effective mass is $lm_e^* + (l-1)m_h^*$. This implies the following conditions on $\{n_i, \sigma_i\}$,

$$l = \sum_{j=0}^{n-1} n_{2j} + \frac{n}{2} + \sum_{j=0}^{n-1} \frac{1-\sigma_{2j+1}}{4}, \quad (11)$$

$$l - 1 = \sum_{j=0}^{n-1} n_{2j+1} + \frac{n}{2} + \sum_{j=1}^{n} \frac{1-\sigma_{2j}}{4}. \quad (12)$$

TABLE I. First values of coefficients $\mathcal{S}(l,n)$ representing the number of nonequivalent orbits for a given mass $m_{e(h)}(l)$ with $2n$ magnetic breakdowns, $1 \leq n \leq 2(l-1)$.

	l					
n	2	3	4	5	6	7
1	2	2	2	2	2	2
2	1	9	23	43	69	101
3		8	68	264	720	1600
4		1	63	610	3080	10925
5			18	584	6132	36980
6			1	228	5950	66374
7				32	2800	64952
8				1	600	34550
9					50	9650
10					1	1305
11						72
12						1

The details of the first-harmonic calculation, Eq. (10), including the previous constraints, Eqs. (11) and (12), are given in Appendix. We found that A_1 is given by the following infinite sum, which takes into account all the possible orbits

$$A_1^{\mathrm{LK}}(e) = \frac{q^2 R(m_e^*)}{m_e^*} + \sum_{l\geq 2} \frac{R[m_e(l)]}{m_e(l)} \times \sum_{n=1}^{2(l-1)} (-1)^n p^{2n} q^{4l-2n-2} \mathcal{S}(l,n), \quad (13)$$

where we defined the combinatorial quantities

$$\mathcal{S}(l,n) = \frac{2}{n} \sum_{i=0}^{n/2} \sum_{j=0}^{i} \sum_{k=0}^{n/2-j} \frac{(-1)^j}{2^{2k}} \binom{n}{2i} \binom{i}{j} \binom{n-2j}{2k} \binom{2k}{k} \times \binom{l+k-1}{l-n+j+k} \binom{l+k-2}{l-n+j+k-1}. \quad (14)$$

These positive integers $\mathcal{S}(l,n)$ count the number of nonequivalent orbits with a given mass $m_{e(h)}(l)$ and for which the quasiparticle is visiting $2n$ successive pockets. In Table I we have reported, for information, the first numbers for increasing values of l from 2 up to 7, using relation (14). For a given l, n is taken from 1 to its maximum value $2(l-1)$.

Finally, the total amplitude for the first harmonic is given by the sum of hole and electron contributions with an overall factor F_0/π,

$$A_1^{\mathrm{LK}} = \frac{F_0}{\pi}[A_1^{\mathrm{LK}}(e) + A_1^{\mathrm{LK}}(h)]. \quad (15)$$

The first-harmonic amplitude is determined by the set of Eqs. (13)–(15). Examples are given in Fig. 6 (solid lines) and

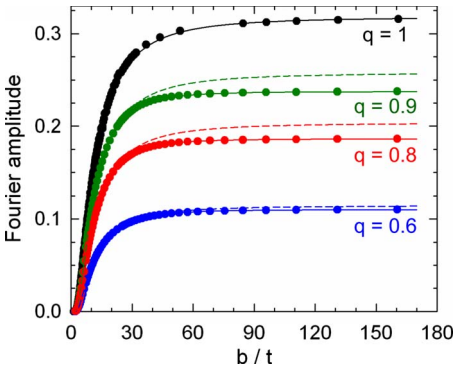

FIG. 6. (Color online) b/t dependence of the first-harmonic amplitude. Solid symbols are deduced from the numerical resolution of Eq. (6). Solid lines correspond to the Lifshits-Kosevich approximation given by Eqs. (13)–(15). Dashed lines correspond to the first-order term [$l=1$ in Eq. (13)]. The effective masses are $m_e=1$ and $m_h=2.5$.

compared to the numerical resolution of the Fourier spectrum of the magnetization taken from Eq. (6) (solid symbols) and for different q values. Since the q value is fixed, these data can be regarded as temperature-dependent amplitudes at a given field. An excellent agreement between numerical results and Eqs. (13)–(15) is observed, even at high magnetic field. Dashed lines in this figure are the contributions of the first-order terms [Eq. (15) reduces to $A_1^{\mathrm{LK}}=q^2F_0[R(m_e^*)/m_e^*+R(m_h^*)/m_h^*]/\pi$ within this approximation]. These terms, which only takes into account the basic orbits with the lowest effective masses (m_e^* and m_h^*) are strongly dominant since only a small difference (less than 10%) is observed in the high b/t range. However, as discussed below, the high-order terms with higher effective masses can have a significant influence on the evaluation of the effective masses from experimental data.

In the case of real experimental data collected on quasi-2D compensated metals, an effective mass m^* is deduced from the temperature dependence of the amplitude of the first harmonic A_1 at a fixed magnetic field. In such a case, it is implicitly assumed that either the effective mass of electron and hole orbits is the same or, oppositely, that only one orbit contributes to the considered Fourier component because the other has a much larger effective mass. In addition, the contribution of high-order orbits ($l>1$) is neglected. Taking into account the Dingle damping factor [see Eq. (8)], we can rewrite the Lifshits-Kosevich formula as,

$$y \propto R_{MB}\frac{e^{-2\pi^2 m^* t^*/b}}{\sinh(2\pi^2 m^* t/b)}, \tag{16}$$

where $y=A_1 b/t$, R_{MB} is the relevant magnetic breakdown damping factor and t^* is the reduced Dingle temperature. If the magnetic field is fixed, Eq. (16) reduces to $y \propto 1/\sinh(2\pi^2 m^* t/b)$. Therefore, the effective mass can be extracted by considering the following combination of derivatives

$$(2\pi^2 m^*)^2 = 2\left[\frac{1}{y}\frac{\partial y}{\partial(t/b)}\right]^2 - \frac{1}{y}\frac{\partial^2 y}{\partial^2(t/b)}. \tag{17}$$

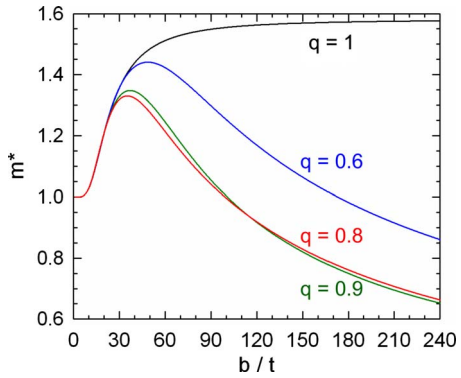

FIG. 7. (Color online) b/t dependence of the effective mass deduced from Eq. (17) with the parameters relevant to data in Fig. 6.

Figure 7 displays the b/t dependence of m^* corresponding to the data in Fig. 6 which stands for a perfect crystal ($t^*=0$). For a given q value, the results are scaled as $m^*/\min(m_e^*,m_h^*)$. For $q=1$, data analysis based on Eq. (17) yields $m^*=\min(m_e^*,m_h^*)$ and $\sqrt{m_e^* m_h^*}$ in the low and high b/t limit, respectively. This point is further supported by considering the mass plot in Fig. 8 which yields a straight line at high t/b.

For $q<1$, a strongly nonmonotonic b/t dependence of m^* is observed in Fig. 7. This behavior is linked to the high-order terms [$l>1$ in Eqs. (13) and (14)]. The q dependence of this behavior is also strongly nonmonotonic since numerous zeroes can arise in the coefficients involved in Eq. (13) as q varies. Nevertheless, the effective mass variations are damped for real crystals with finite Dingle temperature, as demonstrated in Fig. 9 for $q=0.6$ where it is assumed that $t_e^*=t_h^*$ for simplicity. Assuming a fixed magnetic field of 30 T (which yields a breakdown field $B_0=30.6$ T for $q=0.6$), $t^*/b=0.01$ stand for a good crystal with a Dingle temperature $T_D=0.4$ K. Oppositely, $t^*/b=1$, for which m^* is always close to $\min(m_e^*,m_h^*)$ corresponds to an extremely bad crystal for which $\omega_c\tau=b/2\pi m^* t^*$ (where the cyclotron frequency ω_c

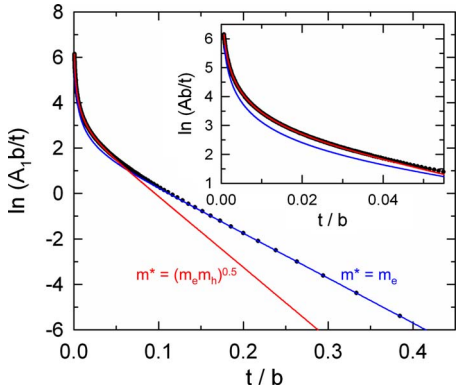

FIG. 8. (Color online) t/b dependence of $y=A_1 b/t$ deduced from Eqs. (13)–(15) for $m_e^*=1$, $m_h^*=2.5$, and $q=1$ (solid symbols) and best fits of Eq. (17) to this data in the low (red solid line) and high (blue solid line) t/b range. The inset displays the low t/b range.

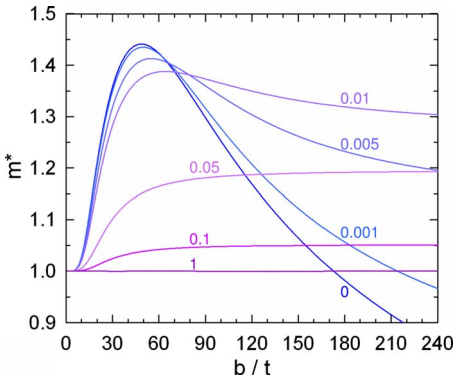

FIG. 9. (Color online) b/t dependence of the effective mass deduced from Eq. (17) for $m_e^*=1$, $m_h^*=2.5$, $q=0.6$ and various values of the Dingle temperature (t^*) indicated on the curves.

$=2\pi\hbar b/m_0 m^* A_0$ in reduced units) is much lower than 1 at experimentally accessible fields.

IV. PROPERTIES OF THE SECOND HARMONIC IN THE CANONICAL ENSEMBLE

In this section, we study the t/b dependence of the second harmonic. Even though an analytical expression is difficult to derive for $q<1$, it is nevertheless possible to obtain some information in the limiting case $q=1$, which has already been considered in a previous study.[21] In particular, we have seen that, within this limit, the free energy ΔF, for a compensated metal, is given by the difference between the grand potentials of the electron and hole bands, respectively,

$$\Delta F = \Omega_e - \Omega_h \simeq -m_e^*\frac{\mu^2}{2} - m_h^*\frac{(\Delta-\mu)^2}{2} + \frac{b^2}{2m_e^*}\sum_{n=1}^{\infty}\frac{(-1)^n}{\pi^2 n^2}R(nm_e^*)\cos\left(2\pi n m_e^*\frac{\mu}{b}\right) + \frac{b^2}{2m_h^*}\sum_{n=1}^{\infty}\frac{(-1)^n}{\pi^2 n^2}R(nm_h^*)\cos\left(2\pi n m_h^*\frac{\Delta-\mu}{b}\right). \quad (18)$$

The chemical potential μ satisfies the self-consistent equation $\partial\Delta F/\partial\mu=0$ given by

$$\mu = \mu_0 + \frac{b}{m_e^*+m_h^*}\sum_{n=1}^{\infty}\frac{(-1)^n}{\pi n}\left[R(nm_h^*)\sin\left(2\pi n m_h^*\frac{\Delta-\mu}{b}\right) - R(nm_e^*)\sin\left(2\pi n m_e^*\frac{\mu}{b}\right)\right]. \quad (19)$$

In the case where the chemical potential is fixed ($\mu=\mu_0$), we can obtain directly the Lifshits-Kosevich expression for $A_2=A_2^{\mathrm{LK}}$ by computing the magnetization $-\partial\Delta F/\partial b$ at fixed μ and extracting the second harmonic,

$$A_2^{\mathrm{LK}} = -\frac{F_0}{\pi}\left[\frac{R(2m_e^*)}{2m_e^*}+\frac{R(2m_h^*)}{2m_h^*}\right]. \quad (20)$$

Otherwise, as discussed above, it is important to keep in mind that the oscillations of the chemical potential are strongly damped in the case where m_e^* and m_h^* have close values. Indeed if we approximate μ by μ_0 at first order in b in the sum terms of Eq. (19), each amplitude of harmonics nF_0 is proportional to $R(nm_h^*)-R(nm_e^*)$ which vanishes when $m_e^*=m_h^*$. It has to be pointed out that in this case, $\mu=\mu_0$ is even the exact solution of the previous Eq. (19), and not simply an approximation.

Since $q=1$, the linear chain is composed of independent and successive electron and hole pockets. We can therefore follow the appendix B of Ref. 21 and the detailed part III of Ref. 12 to extract analytically (for small field values) the amplitude of the second harmonic from Eqs. (18) and (19). The oscillatory part of the magnetization is given by $M_{osc}=-\partial\Delta F/\partial b=x^2\partial\Delta F/\partial x$ (we remind that $x=1/b$). We then introduce the periodic function

$$G(x) = \sum_{n=1}^{\infty}\frac{(-1)^n}{\pi n}[R(nm_h^*)-R(nm_e^*)]\sin(2\pi n F_0 x) \quad (21)$$

so that the chemical potential, Eq. (19), can be expressed as $\mu=\mu_0+bG(x)/(m_e^*+m_h^*)$, and the magnetization

$$M_{osc} \approx -\frac{1}{(m_e^*+m_h^*)}G(x)G'(x) + \frac{1}{2}\sum_{n=1}^{\infty}\frac{(-1)^n}{\pi^2 n^2}\Re\left\{\frac{R(nm_e^*)}{m_e^*}\frac{\partial}{\partial x}\exp[2i\pi n F_0 x + 2i\pi n w_e G(x)] + \frac{R(nm_h^*)}{m_h^*}\frac{\partial}{\partial x}\exp(2i\pi n F_0 x - 2i\pi n w_h G(x)\right\} \quad (22)$$

with $w_{e(h)}=m_{e(h)}^*/(m_e^*+m_h^*)$. We make the further approximation in the exponential parts of Eq. (22), and which is valid at low temperature, that $G(x)$ can be truncated to the first term $G(x)\approx[R(m_e^*)-R(m_h^*)]\sin(2\pi F_0 x)/\pi$ so that

$$e^{2i\pi n w_{e(h)}G(x)} = \sum_{m=-\infty}^{\infty} J_m(n\alpha_{e(h)})\exp(2i\pi m F_0 x), \quad (23)$$

where $\alpha_{e(h)}=2m_{e(h)}[R(m_e^*)-R(m_h^*)]/(m_e^*+m_h^*)$ and J_m are the Bessel functions of integer order. Putting expression (23) into expression (22), we then select, in order to isolate the second harmonics, integers such that $n+m=\pm 2$ and $n-m=\pm 2$ for the electron and hole contributions, respectively. Expanding the magnetization in terms of Fourier components $M_{osc}=-A_1\sin(2\pi F_0)+A_2\sin(4\pi F_0)+\cdots$, we find that the coefficient A_2 satisfies the relation

$$\frac{\pi A_2}{2F_0} = -\frac{[R(m_h^*) - R(m_e^*)]^2}{2(m_e^* + m_h^*)} + \sum_{n\geq 1} \frac{\{R[(n+2)m_h^*] - R[(n+2)m_e^*]\}[R(nm_h^*) - R(nm_e^*)]}{n(n+2)(m_e^* + m_h^*)}$$
$$- \sum_{n\geq 1} \frac{1}{n^2}\left\{\frac{R(nm_e^*)}{m_e^*}[J_{n-2}(n\alpha_e) - J_{n+2}(n\alpha_e)] + \frac{R(nm_h^*)}{m_h^*}[J_{n-2}(n\alpha_h) - J_{n+2}(n\alpha_h)]\right\}. \quad (24)$$

This expression is quite different from Eq. (20) relevant to the Lifshits-Kosevich model, except in the case where the two masses are equal. In Fig. 10 are plotted the t/b dependence of A_2 deduced from Eq. (20), with the same parameters as in Fig. 6, and Eq. (24) together with the numerical results obtained by solving directly the spectrum, Eq. (2), and extracting the second-harmonic amplitude for different values of q (see Sec. II).

For $q=1$, taking into account the oscillations of the chemical potential, Eq. (24) agrees well with numerical results within a large domain of t/b. Remarkably, as evidenced in Fig. 10, whatever the q value is, the amplitude vanishes at the same t/b value depending on the ratio of the two effective masses only (see the inset of Fig. 10. This behavior is strikingly different from that of A_1, considered in previous section, for which no singularity is observed. This reflects the fact that the deviation from the Lifshits-Kosevich approximation appears only in the second harmonic.

V. SUMMARY AND CONCLUSION

The spectrum for one-dimensional chain of compensated orbits has been calculated. As it is the case for two isolated orbits, the field-dependent oscillations of the chemical potential are weaker than in the case of two electron-type orbits

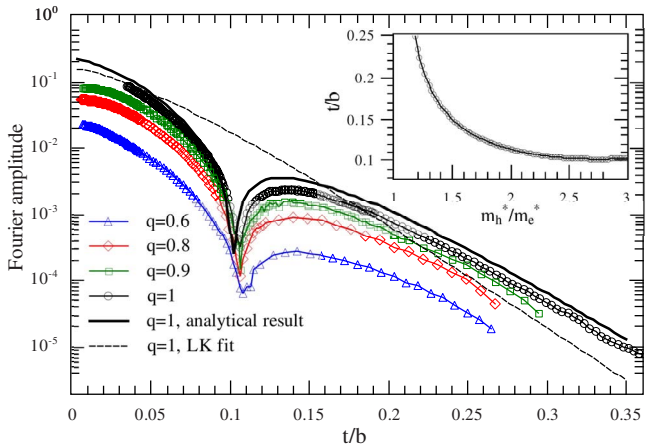

FIG. 10. (Color online) t/b dependence of the second-harmonic amplitude A_2 for various q values. Solid symbols and solid line correspond to the numerical resolution of Eq. (6) and to the solution of approximation, Eq. (24), for $q=1$, respectively. Here $m_e^*=1$ and $m_h^*=5/2$. Dotted line corresponds to the LK approximation formula for the second harmonic [see Eq. (20)] and for $q=1$. In the insert is plotted the critical value of t/b at which A_2 vanishes as function of the ratio m_h^*/m_e^*.

(see the inset of Fig. 4), especially when the two effective masses have close values. It appears from the analysis of the numerical resolution of Landau levels, including the electron-hole band interaction, that the Lifshits-Kosevich semiclassical formalism can be applied for the first harmonic, provided magnetic breakdown orbits, although with higher effective masses, are taken into account. The resulting high-order terms [$l>1$ in Eqs. (13) and (14)] can lead to apparent temperature-dependent effective mass for clean crystals in the high b/t limit in the case where only one effective mass is considered for the data analysis, as it is usually done. On the contrary, strong deviation from the Lifshits-Kosevich behavior is observed for the second harmonic. The main feature of this latter component being the zero amplitude occurring at a t/b value depending only on the effective-mass ratio m_h^*/m_e^*. As seen in the inset of Fig. 10, the larger this value is, the closer the two masses are. This feature could provide a straightforward method for determining the effective-mass ratio since the heaviest mass contribution to the first-harmonic amplitude is generally hidden by the amplitude of the lightest one, at least at low b/t value. The strong deviations of the second harmonic from the Lifshits-Kosevich behavior are reminiscent of data reported for systems whose Fermi surface is composed of an electron pocket with a one-dimensional reservoir,[15] or in the direct observation[24] of spin-zero anomaly in the organic conductor β''-$(BEDT\text{-}TTF)_2SF_5CH_2CF_2SO_3$ where an accurate treatment of the second harmonic, similar to the previous section calculation and which includes the oscillating potential effect, solves the discrepancy between experimental data and the fit by Lifshits-Kosevich formula. Finally, it can be remarked that the studied 1D chain does not yield frequency combinations. Only harmonics of the fundamental frequency are observed. In a next step, it is planned to consider 2D networks of compensated orbits which account for the Fermi surface of many organic metals and are known to give rise to such phenomenon.

APPENDIX

In this appendix we derive in details the computation of the first harmonic A_1 from Eq. (10) in Sec. III, within the Lifshits-Kosevich and Falicov-Stachowiak theory framework. The constrained sums, Eqs. (11) and (12), can be transformed using two Kronecker integrals around the complex unit circle

$$A_1^{\mathrm{LK}}(e)=\frac{q^2R(m_e^*)}{m_e^*}+\sum_{l\geq 2}\frac{R[m_e(l)]}{m_e(l)}\times\sum_{n=1}^{2(l-1)}\frac{(-1)^n}{n}\sum_{\{n_i,\sigma_i\}}p^{2n}q^n e^{K\Sigma_{j=1}^{2n}\sigma_j}\oint\frac{dz}{2i\pi z}\oint\frac{dz'}{2i\pi z'}\times q^{2\Sigma_{j=0}^{n-1}n_{2j}z^{-l+\Sigma_{j=0}^{n-1}n_{2j}+n/2+\Sigma_{j=0}^{n-1}1-\sigma_{2j+1}/4}}\times q^{2\Sigma_{j=0}^{n-1}n_{2j+1}z'^{-l+1+\Sigma_{j=0}^{n-1}n_{2j+1}+n/2+\Sigma_{j=1}^{n}1-\sigma_{2j}/4}}. \quad \text{(A1)}$$

The sums over the $\{n_i=0,\ldots,\infty\}$ can be performed exactly since q is less than unity. We obtain

$$A_1^{\mathrm{LK}}(e)=\frac{q^2R(m_e^*)}{m_e^*}+\sum_{l\geq 2}\frac{R[m_e(l)]}{m_e(l)}\times\sum_{n=1}^{2(l-1)}\frac{(-1)^n}{n}\sum_{\{\sigma_i\}}p^{2n}q^n e^{K\Sigma_{i=1}^{2n}\sigma_i}\oint\frac{dz}{2i\pi z}\oint\frac{dz'}{2i\pi z'}\times\frac{z^{-l+3n/4}}{(1-q^2z)^n}\frac{1}{z^{\Sigma_{j=0}^{n-1}\sigma_{2j+1}/4}}\frac{z'^{-l+1+3n/4}}{(1-q^2z')^n}\frac{1}{z'^{\Sigma_{j=1}^{n}\sigma_{2j}/4}}. \quad \text{(A2)}$$

The condition for a closed path is given by $\Sigma_{j=1}^{2n}y_j=0$, with the periodic conditions $y_0=y_{2n}$, which imposes in the previous sum the introduction of another Kronecker function. The previous quantities depending on $\sigma_i=y_iy_{i-1}$ can be rewritten in term of the y_i's only. Using the fact that $e^K=1/\sqrt{q}$, the sum over the terms involving these variables is given by the quantity

$$Z_0=\sum_{\{y_i=\pm 1\}}\int_0^{2\pi}\frac{d\alpha}{2\pi}e^{i\alpha\Sigma_{j=1}^{2n}y_j}\times\prod_{j=0}^{n-1}(zq^2)^{-y_{2j}y_{2j+1}/4}(z'q^2)^{-y_{2j+1}y_{2j+2}/4}. \quad \text{(A3)}$$

This is the partition function for a one-dimensional periodic Ising model with an imaginary field and alternate complex coupling. Setting the 2×2 transfer matrices $P_{yy'}=(zq^2)^{-yy'/4}e^{i\alpha(y+y')/2}$ and $P'_{yy'}=(z'q^2)^{-yy'/4}e^{i\alpha(y+y')/2}$, Z_0 can be written as a trace over the product of operators $(PP')^n$,

$$Z_0=\mathrm{Tr}(PP')^n=\lambda_+^n+\lambda_-^n, \quad \text{(A4)}$$

where $\lambda_\pm$ are the eigenvalues of the matrix PP'. The amplitude can then be written as

$$A_1^{\mathrm{LK}}(e)=\frac{q^2R(m_e^*)}{m_e^*}+\sum_{l\geq 2}\frac{R[m_e(l)]}{m_e(l)}\times\sum_{n=1}^{2(l-1)}\frac{(-1)^n}{n}p^{2n}q^n\oint\frac{dz}{2i\pi z}\oint\frac{dz'}{2i\pi z'}\times\frac{z^{-l+3n/4}}{(1-q^2z)^n}\frac{z'^{-l+1+3n/4}}{(1-q^2z')^n}Z_0. \quad \text{(A5)}$$

It is useful to express complex vectors $z=e^{i\theta}$ and $z'=e^{i\theta'}$ by their angles θ and θ'. Also, setting $\zeta=\sqrt{q}e^{i\theta/4}$, $\zeta'=\sqrt{q}e^{i\theta'/4}$, $\bar{\zeta}=1/\zeta$, and $\bar{\zeta}'=1/\zeta'$, we can express the eigenvalues as

$$\lambda_\pm=\nu(\theta,\theta',\alpha)\pm\sqrt{\nu^2+\eta(\theta,\theta')},$$

$$\nu(\theta,\theta',\alpha)=\bar{\zeta}\bar{\zeta}'\cos(2\alpha)+\zeta\zeta',$$

$$\eta(\theta,\theta')=-(\zeta^2-\bar{\zeta}^2)(\zeta'^2-\bar{\zeta}'^2)=-(1-q^2z)(1-q^2z')/(q^2\sqrt{zz'}). \quad \text{(A6)}$$

Then

$$Z_0=2\sum_{i=0}^{n/2}\sum_{j=0}^{i}\binom{n}{2i}\binom{i}{j}\nu^{n-2j}\eta^j=2\sum_{i=0}^{n/2}\sum_{j=0}^{i}\sum_{k=0}^{n-2j}\binom{n}{2i}\binom{i}{j}\binom{n-2j}{k}(\zeta\zeta')^{n-2j-2k}\eta^j\cos^k(2\alpha), \quad \text{(A7)}$$

where we introduced binomial coefficients $\binom{n}{k}=n!/k!(n-k)!$. In the last line, we can perform the integral over α of the integrand $\cos^k(2\alpha)$. The resulting integral is not zero only for k even

$$\int_0^{2\pi}\frac{d\alpha}{2\pi}\cos^{2k}(2\alpha)=\frac{1}{2^{2k}}\binom{2k}{k}. \quad \text{(A8)}$$

We finally obtain

$$Z_0=2\sum_{i=0}^{n/2}\sum_{j=0}^{i}\sum_{k=0}^{n/2-j}\binom{n}{2i}\binom{i}{j}\binom{n-2j}{2k}\binom{2k}{k}\frac{(\zeta\zeta')^{n-2j-4k}\eta^j}{2^{2k}}.$$

The amplitude A_1^{LK} can be rearranged using the previous results like

$$A_1^{\mathrm{LK}}(e)=\frac{q^2R(m_e^*)}{m_e^*}+\sum_{l\geq 2}\frac{R[m_e(l)]}{m_e(l)}\times\sum_{n=1}^{2(l-1)}2\frac{(-1)^n}{n}p^{2n}\sum_{i=0}^{n/2}\sum_{j=0}^{i}\sum_{k=0}^{n/2-j}\binom{n}{2i}\binom{i}{j}\binom{n-2j}{2k}\times\binom{2k}{k}\frac{(-1)^j}{2^{2k}}\times\oint\frac{dz}{2i\pi z}\oint\frac{dz'}{2i\pi z'}\times\frac{z^{-l+n-j-k}}{(1-q^2z)^{n-j}}\frac{z'^{-l+1+n-j-k}}{(1-q^2z')^{n-j}}q^{2n-4j-4k}. \quad \text{(A9)}$$

To compute the last two complex integrals, we use the relation for any positive integers (α,β)

$$\oint\frac{dz}{2i\pi z}\frac{z^{-\alpha}}{(1-q^2z)^\beta}=\binom{\beta+\alpha-1}{\alpha}q^{2\alpha}. \quad \text{(A10)}$$

Then we obtain the main result, Eq. (13), with the combinatorial integer coefficients given in Eq. (14).

*fortin@lpm.u-nancy.fr
†alain.audouard@lncmi.cnrs.fr

[1] A. Pippard, Proc. R. Soc. London, Ser. A **270**, 1 (1962).
[2] R. Chambers, Proc. Phys. Soc. **88**, 701 (1966).
[3] M. H. Cohen and L. M. Falicov, Phys. Rev. Lett. **7**, 231 (1961).
[4] J.-Y. Fortin, J. Bellissard, M. Gusmão, and T. Ziman, Phys. Rev. B **57**, 1484 (1998).
[5] L. M. Falicov and H. Stachowiak, Phys. Rev. **147**, 505 (1966).
[6] A. S. Alexandrov and A. M. Bratkovsky, Phys. Rev. Lett. **76**, 1308 (1996).
[7] P. S. Sandhu, J. H. Kim, and J. S. Brooks, Phys. Rev. B **56**, 11566 (1997).
[8] J.-Y. Fortin and T. Ziman, Phys. Rev. Lett. **80**, 3117 (1998).
[9] V. M. Gvozdikov, Y. V. Pershin, E. Steep, A. G. M. Jansen, and P. Wyder, Phys. Rev. B **65**, 165102 (2002).
[10] T. Champel, Phys. Rev. B **65**, 153403 (2002).
[11] K. Kishigi and Y. Hasegawa, Phys. Rev. B **65**, 205405 (2002).
[12] J. Y. Fortin, E. Perez, and A. Audouard, Phys. Rev. B **71**, 155101 (2005).
[13] N. Harrison, A. House, I. Deckers, J. Caulfield, J. Singleton, F. Herlach, W. Hayes, M. Kurmoo, and P. Day, Phys. Rev. B **52**, 5584 (1995).
[14] P. Sandhu, G. Athas, J. Brooks, E. Haanappel, J. Goettee, D. Rickel, M. Tokumoto, N. Kinoshita, T. Kinoshita, and Y. Tanaka, Surf. Sci. **361-362**, 913 (1996)
[15] N. Harrison, R. Bogaerts, P. H. P. Reinders, J. Singleton, S. J. Blundell, and F. Herlach, Phys. Rev. B **54**, 9977 (1996).
[16] T. Champel, Phys. Rev. B **64**, 054407 (2001).
[17] R. Rousseau, M. Gener, and E. Canadell, Adv. Funct. Mater. **14**, 201 (2004).
[18] C. Proust, A. Audouard, L. Brossard, S. Pesotskii, R. Lyubovskii, and R. Lyubovskaya, Phys. Rev. B **65**, 155106 (2002).
[19] D. Vignolles, A. Audouard, L. Brossard, S. Pesotskii, R. Lyubovskii, M. Nardone, E. Haanappel, and R. Lyubovskaya, Eur. Phys. J. B **31**, 53 (2003).
[20] A. Audouard, D. Vignolles, E. Haanappel, I. Sheikin, R. B. Lyubovskii, and R. N. Lyubovskaya, Europhys. Lett. **71**, 783 (2005).
[21] J. Y. Fortin and A. Audouard, Phys. Rev. B **77**, 134440 (2008).
[22] T. G. Prokhorova, S. S. Khasanov, L. V. Zorina, L. I. Buravov, V. A. Tkacheva, A. A. Baskakov, R. B. Morgunov, M. Gener, E. Canadell, R. P. Shibaeva, and E. B. Yagubskii, Adv. Funct. Mater. **13**, 403 (2003).
[23] W. Kang, K. Behnia, D. Jérome, L. Balicas, E. Canadell, M. Ribault, and J. M. Fabre, Europhys. Lett. **29**, 635 (1995).
[24] J. Wosnitza, V. M. Gvozdikov, J. Hagel, O. Ignatchik, B. Bergk, P. J. Meeson, J. A. Schlueter, H. Davis, R. W. Winter, and G. L. Gard, New J. Phys. **10**, 083032 (2008).